

## THE STRUCTURE AND EVOLUTION OF CIRCUMBINARY DISKS IN CATAclySMIC VARIABLE SYSTEMS

GUILLAUME DUBUS<sup>1</sup>, RONALD E. TAAM<sup>2</sup>, AND H. C. SPRUIT<sup>3</sup>

<sup>1</sup>California Institute of Technology, MC 130-33, Pasadena, CA 91125

<sup>2</sup>Department of Physics & Astronomy, Northwestern University, Evanston, IL 60208

<sup>3</sup>Max-Planck-Institut für Astrophysik, Postfach 1317, D-85741 Garching, Germany

*Draft version October 29, 2018*

### ABSTRACT

We investigate the structure and evolution of a geometrically thin viscous Keplerian circumbinary (CB) disk, using detailed models of their radiative/convective vertical structure. We use a simplified description for the evolution of the cataclysmic binary and focus on cases where the circumbinary disk causes accelerated mass transfer ( $\gtrsim 10^{-8} M_{\odot} \text{ yr}^{-1}$ ). The inner edge of the disk is assumed to be determined by the tidal truncation radius and the mass input rate into the disk is assumed to be a small fraction ( $10^{-5}$ –0.01) of the mass transfer rate. Under the action of the viscous stresses in the disk the matter drifts outward with the optically thick region extending to several AU. The inner part of the disk is cool with maximum effective temperatures  $\lesssim 3,000$  K while the outermost parts of the disk are  $\lesssim 30$  K and optically thin. We calculate the effects of thermal instability on a sufficiently massive CB disk. It leads to outbursts reminiscent of those in thermally unstable accretion disks, with the instability remaining confined to the inner regions of the CB disk. However, for most of the evolutionary sequences the surface densities required to trigger instability are not reached. The spectral energy distributions from circumbinary disks are calculated, and the prospects for the detection of such disks in the infrared and submm wavelength regions are discussed.

*Subject headings:* binaries: close — stars: evolution — stars: cataclysmic variables

### 1. INTRODUCTION

Over the last decade evidence has been accumulating suggesting the presence of gaseous matter beyond the orbit of the components in cataclysmic variable binary systems (CVs). Its existence has been inferred from P-Cygni profiles in nova-like variables, super soft sources, and dwarf novae in outburst (see, for example, Deufel et al. 1999). In addition, the observation of narrow widths of single-peaked emission lines in SW Sex stars (see Thorstensen et al. 1991; Hellier 2000) and low velocity spectral features in AM CVn which do not follow the orbital motion of the binary system (see Solheim & Sion 1994) provide further support for this interpretation. Such a gaseous component may take the form of an extended shell or a flattened distribution of matter surrounding the binary system. Assuming that some fraction of this matter remains bound to the system and condenses into the orbital plane, in analogy to the compression of a radiation-driven wind into the equatorial plane in Be-stars (Bjorkman & Cassinelli 1993, Bjorkman & Wood 1995), a circumbinary disk may form. The presence of such a CB disk, as proposed by Spruit & Taam (2001), can provide an attractive explanation for some of the discrepancies between observations and the current theory of evolution of CVs.

The importance of a CB disk for the evolution of a CV lies in the angular momentum it can extract from the binary, leading to mass transfer rates exceeding those due to magnetic braking and/or gravitational radiation. The binary exerts gravitational torques on the external disk, thereby transferring some of its orbital angular momentum. If some fraction of the mass lost from the main sequence-like secondary of the system forms a CB disk, a

feedback process can operate to accelerate the binary evolution. As shown in the detailed computations by Taam & Spruit (2001) the evolution of the system can be significantly accelerated and the mass transfer rate from the secondary towards the white dwarf,  $\dot{M}_2$ , elevated to rates as high as  $10^{-7} M_{\odot} \text{ yr}^{-1}$ .

In previous studies, we have focused on the response of the mass losing component and on the evolution of the binary system resulting from the influence of the CB disk, using a one zone approximation for its vertical structure. Here, we report on the results of detailed numerical calculations for the vertical structure and radial evolution of such disks surrounding a model CV. In order to determine the observability of such disks, their spectral energy distributions are also presented. The assumptions of the model computations are described in the next section. In §3 we describe the evolution of a CB disk neglecting angular momentum losses from the binary system. Results with the binary evolution taken into account are shown in §4 and several spectral energy distributions for some illustrative systems are presented in §5. We summarize and conclude in the last section.

### 2. MODEL

We assume that the CB disk is axisymmetric and geometrically thin such that matter rotates at the Keplerian speed. The formulation of the equations for mass, angular momentum, and energy transport is as described in Hameury et al. (1998). Models for the radiative/convective vertical structure have been calculated and tabulated in a grid for a range of radii, mid-plane temperatures, and column densities. The global structure

and evolution of the disk follows from the coupling of this grid to the time dependent transport of mass, energy, and angular momentum in the radial direction. The viscous stress tensor,  $\tau_{r\phi}$ , is assumed to be equal to  $\alpha P$  where  $\alpha$  is the viscosity parameter introduced by Shakura & Sunyaev (1973) and  $P$  is the local pressure in the disk. The calculations of the disk differ from those of Taam & Spruit (2001) where the vertical structure of the disk was calculated in a one zone approximation. Furthermore, we take into account departures from local thermal equilibrium and include convective energy transport. The latter is treated in the mixing length approximation with the ratio of mixing length to pressure scale height taken to be equal to 1.5, where the functional form for the pressure scale height is chosen to ensure that it does not exceed the vertical scale height.

Optically thin regions above the disk photosphere are included in the computation and are treated in the grey approximation. The input physics includes an equation of state of matter in which the ionization/dissociation balance of hydrogen is taken into account. The opacities are taken from Bell et al. (1997) and include contributions from iron poor opacities at temperatures ( $T \lesssim 1500$  K) where dust particles exist (Henning & Stognienko 1996). It is assumed that the composition of the material corresponds to a solar mix ( $X = 0.7$ ,  $Y = 0.28$ , and  $Z = 0.02$ ).

The boundary conditions are formulated such that both the inner radius and outer radius of the disk can vary in time. At the inner radius, it is assumed that the mass input rate into the CB disk is a constant fraction of the mass transfer rate from the secondary  $\dot{M}_1 = -\delta\dot{M}_2$ . Although the mass input into the disk may extend over a range of radii, we have adopted the simplest approach and assumed that the mass is deposited at its innermost edge. The condition that this input mass flux is carried outward by viscous diffusion serves as an inner boundary condition, which is formulated as a relation between  $\Sigma$  and its gradient. The specific angular momentum of the mass fed into the disk is taken to be equal to that of a Kepler orbit at the inner edge. The mass deposited is thus neutral in an angular momentum sense. In addition, it is assumed that the radial temperature gradient vanishes. Our treatment differs from that adopted in Pringle (1991) in that we have a mass input into the disk which is absent in the formulation developed by Pringle (1991). In the latter equivalent approach, the radial velocity at the inner edge is assumed to vanish. The column density and the mass outflow rate at the outer boundary are set to  $10^{-2}$  g cm $^{-2}$  and zero respectively. With these treatments of the boundaries, the disk structure and evolutionary equations are solved in a fully implicit fashion on an adaptive grid (typically with 400 zones). For a full description of the numerical method, see Hameury et al. (1998).

Since the primary focus of this investigation is on the structure of the CB disk, the evolution of the binary system is treated in a simplified approximation wherein the response of the mass losing star is modeled assuming homology (Spruit & Ritter 1983; see also Spruit & Taam 2001). The mass transfer process is assumed to be conservative. That is, a very small fraction,  $\delta < 0.01$ , of the mass lost from the donor star, which itself is assumed to be small compared to the mass transferred to its companion,

is assumed to be deposited into the CB disk.

Angular momentum loss associated with magnetic braking is assumed to take place on a fixed timescale  $t_w$ . The contribution of the CB disk to the angular momentum loss from the binary is given by the viscous torque at the inner edge of the disk,

$$\dot{J}_d = 3\pi(R_i/a)^{1/2}\Omega_0 a^2 \nu_i \Sigma_i, \quad (1)$$

where  $\Omega_0$  is the orbital frequency of the binary system,  $a$  is the orbital separation of the binary components, and  $R_i$ ,  $\nu_i$ , and  $\Sigma_i$  are the radius, viscosity, and column density at the inner edge of the CB disk respectively. The evolution of the system follows from the total angular momentum loss, (see Spruit & Taam 2001):

$$-\dot{J}/J = t_w^{-1} + 3\pi(R_i/a)^{1/2}(1+q)/M_2 \nu_i \Sigma_i \quad (2)$$

It is assumed that the gravitational torque is concentrated near the inner edge of the disk and that the radius of the inner edge is approximately equal to 1.7 times the orbital separation. This latter assumption is based on the work of Artymowicz & Lubow (1994) who show that the ratio of the inner radius of the CB disk to the orbital separation is relatively insensitive to the mass ratio of the binary system,  $q$ , due to the steep decrease of the tidal torques with distance.

### 3. CB DISKS IN NON-EVOLVING SYSTEMS

As a first step we computed several CB disk models in which we neglected all the angular momentum losses from the binary system. The binary evolution is thereby frozen with the inner radius  $R_i$  and mass input rate  $\dot{M}_1$  (instead of  $\delta$ ) set as constant parameters. Our calculations start with a very low density ( $\Sigma = 0.01$  g cm $^{-2}$ ) ring of matter at the inner edge, and we follow the expansion of the disk as matter gradually piles up and diffuses outwards.

Fig. 1 is an example of the evolution of the column density at the inner radius,  $\Sigma_i$ , and of the outer radius,  $R_d$ , for a CB disk with  $\alpha = 0.001$ ,  $R_i = 10^{11}$  cm,  $\dot{M}_1 = -10^{14}$  g s $^{-1}$  (the negative value indicating mass is flowing away from the binary) and a binary mass  $M$  of 1  $M_\odot$ . The outer disk radius as shown in Fig. 1 is defined as the radius at which the disk becomes optically thin ( $\tau = 1$ ). After a transitory period lasting at most a few hundred years (viscous timescale of the inner edge), both  $\Sigma_i$  and  $R_d$  increase gradually in a roughly self-similar, power law-like fashion. This behaviour is independent of the initial setup and, to a large extent, independent of the outer boundary conditions on  $\dot{M}$  and  $\Sigma$ . Increasing the mass input rate speeds up the evolution with higher values of  $\Sigma_i$  reached sooner. Changing  $\alpha$  has a weaker influence with lower viscosities leading to slightly higher values of  $\Sigma_i$ . Both of these effects can be seen in Figs. 3-6 which take the binary evolution into account and are discussed in the next section.

The evolution of the column density, mid-plane temperature, effective temperature, ratio of scale height to radius, and mass flow rate are illustrated as a function of radius and time in Fig. 2. It is evident that the column densities continually increase at a given radius and reach densities as high as  $10^4$  g cm $^{-2}$  at the inner disk edge. The point at which the optical depth equals unity (denoted as a solid dot), corresponding to  $R_d$  in Fig. 1, also increases with time and the optically thick disk reaches a size of about 10

AU at the end of the calculation. The mid-plane temperatures (solid line) and the effective temperatures (dashed line) both increase with time, reflecting the increasing surface density and energy dissipation in the disk associated with the increasing mass flow rate. The mid-plane (effective) temperatures decrease monotonically with distance, from 10000 (3000) K in the innermost regions to 20 (10) K where the disk becomes optically thin. However, we note that such densities and temperatures are reached only after a Hubble time, at which point the neglect of angular momentum losses from the binary is not realistic. The disk remains geometrically thin throughout the evolution, with the ratio of pressure scale height to radius in the optically thick region,  $H/R$ ,  $< 0.05$ . We find that  $H/R$  does not increase uniformly with radius, so that the outer disk region is in the shadow of the inner region, reminiscent of the protostellar circumstellar disks studied by Bell et al. (1997).

The simple self-similar CB disk model of Spruit & Taam (2001), which assumes that the viscosity is a linear function of  $R$  only,  $\nu = \nu_i(R/R_i)$ , gives for the inner regions of the disk:

$$\Sigma(R, t) \approx \left(\frac{t}{t_{vi}}\right)^{1/2} \frac{(-\dot{M}_i)}{3\pi\nu_i} \left(\frac{R}{R_i}\right)^{-3/2} \quad (3)$$

where  $t_{vi} = R_i^2/\nu_i$  is the viscous timescale at the inner edge of the disk. This implies a scaling for  $\Sigma_i \propto \dot{M}_i/\sqrt{\alpha}$ , which we find to be roughly reproduced by the numerical results (see e.g. the early evolution of the disks in Figs. 5-6).

#### 4. CB DISKS IN EVOLVING SYSTEMS

Evolutionary sequences were calculated for model CV systems consisting of a secondary component of  $0.55 M_\odot$  and a primary white dwarf component of  $0.95 M_\odot$ . The disk calculations were performed for several fractional mass input rates into the CB disk  $\delta \lesssim 0.01$ , viscosity parameters  $\alpha \lesssim 0.01$ , and time scales for angular momentum loss by magnetic braking  $t_w \lesssim 10^{10}$  yrs.

##### 4.1. Acceleration of the binary evolution

The results of an evolutionary sequence with parameter values  $\delta = 0.005$ ,  $t_w = 2 \times 10^8$  years, and  $\alpha = 0.001$  are illustrated in Figs. 3 and 4. The CB disk initially evolves in the same fashion as described in the previous section. Angular momentum losses by magnetic braking then start changing the system parameters and the system evolves in a standard way, with  $-\dot{M}_i$  decreasing together with the mass of the secondary. The CB torque begins to dominate the evolution at  $t \approx 20$  Myr, when the mass input rate into the CB disk is approximately at its minimum,  $\dot{M}_i \approx -3 \times 10^{-11} M_\odot \text{ yr}^{-1}$  ( $\dot{M}_2 \approx 6 \times 10^{-9} M_\odot \text{ yr}^{-1}$ ). The mass input rate is now proportional to the surface density since  $\dot{M}_i/M_2 \sim \dot{J}_i/J \sim -(\nu\Sigma)_i/M_2$ , leading to a runaway on a timescale comparable to that on which the CB torque becomes dominant (Spruit & Taam 2001). The acceleration is manifest in Fig. 3 as an abrupt increase of  $-\dot{M}_i$  to  $\gtrsim 10^{-9} M_\odot \text{ yr}^{-1}$ , leading to an increase in the orbital period as a result of the tendency for the secondary to expand as it departs significantly from thermal equilibrium.

By the end of the calculation at  $t \approx 65$  Myr the orbital period is  $\sim 20$  hr and the secondary has  $M_2 \approx 0.03 M_\odot$ .

The response of the star to mass loss certainly deviates from homology during the runaway but there is little doubt that it will end with the dissolution of the secondary. Qualitatively similar results were obtained by Taam & Spruit (2001).

##### 4.2. Influence of the different parameters

The influence of changing  $\alpha$  is also shown in Fig. 3. The CB torque becomes dominant when  $\dot{J}_d \gtrsim \dot{J}_w$ . Combining Eq. 1-3, we find this happens when (Spruit & Taam 2001)

$$\dot{J}_d/J \sim (t/t_{vi})^{1/2} \dot{M}_i/M_2 \sim -t_w^{-1} \quad (4)$$

For a given magnetic braking torque and  $\dot{M}_i$ , the disk torque dominates at  $t \propto t_{vi} \propto 1/\alpha$ . This scaling is consistent with the numerical results of Fig. 3. Note that for very low values of  $\alpha$  ( $\lesssim 0.0001$  for  $\delta = 0.005$  and  $t_w = 0.2$  Gyr) the CB torque would be entirely negligible during the course of the evolution. It should be pointed out that we have implicitly assumed that  $\alpha$  is constant throughout the disk. It is possible that  $\alpha$  may decrease significantly at large radii (see Gammie & Menou 1998) where the magnetic Reynolds number is decreased below values necessary for a magnetic dynamo to operate. In this case, the size and the properties of the outer disk would be modified from that calculated here. However, the extent of the magnetically decoupled region is model dependent as it is very sensitive to the ionization fraction in the disk (see Fromang, Terquem, & Balbus 2002).

Changing the magnetic braking timescale  $t_w$  changes  $\dot{M}_i$  since the initial rate is set by  $\dot{M}_2/M_2 \sim \dot{J}/J \approx t_w^{-1}$  (Eq. 2). Using this in Eq. 4, we find the CB torque should thus start dominating the evolution at roughly the same time regardless of  $t_w$ . This is confirmed by the calculations shown in Fig. 5 in which the disk torque dominates after  $t \approx 20$  Myrs for  $t_w = 0.2, 1$  and  $5$  Gyrs. Note that  $\Sigma_i$  at  $t \approx 20$  Myrs decreases with increasing  $t_w$  since  $\Sigma_i \propto -\dot{M}_i \propto t_w^{-1}$  during the early magnetic braking-dominated evolution. The conditions for the runaway should be independent of  $t_w$  and we indeed find the disks in Fig. 5 to have similar properties when it occurs ( $\Sigma_i \approx 40000 \text{ g cm}^{-2}$ ,  $R_d \approx 10 \text{ AU}$ ).

Fig. 6 illustrates the influence of changing the fraction of the mass transferred to the CB disk. For  $\delta \gtrsim 0.01$  the system dissolves in  $\lesssim 1$  Myr suggesting that systems with high values of  $\delta$  are unlikely to be observed. The timescale on which the disk torque dominates dramatically increases as  $\delta$  becomes smaller. The effect is much stronger than decreasing  $\alpha$  as already noted by Taam & Spruit (2001). For values of  $\delta \lesssim 0.0001$  the disk torque becomes important on timescales longer or comparable to the magnetic braking timescale  $t_w$ . The secondary has then already lost most of its mass so that the CB disk has no impact on the binary evolution. Being smaller and less massive, the CB disk is also fainter and more difficult to detect (see §5).

Taam & Spruit (2001), using a detailed evolutionary code for the secondary but a simpler disk model, found that the CB torque was negligible when  $\delta \lesssim 0.01$ . The present calculations indicate that disks formed with  $\delta \gtrsim 0.0001$  can still influence the binary. The discrepancy can be traced to the assumptions made in the different models. In Taam & Spruit (2001), the column densities at the inner

edge of the disk are very close to the lower turning point of the S curve ( $\Sigma_{\max} \approx 4000 \text{ g cm}^{-2}$  at  $R = 10^{11} \text{ cm}$  with  $M = 1 M_{\odot}$  and  $\alpha = 0.001$ , see Fig. 1 of Taam & Spruit). The specific interpolation scheme between the two stable branches which they used forces the column density to stagnate around  $\Sigma_{\max}$  once this value is reached. The detailed vertical structure computations, which include convection, show that the actual value of  $\Sigma_{\max}$  is an order of magnitude higher than in the one zone radiative model ( $\Sigma_{\max} \approx 40000 \text{ g cm}^{-2}$  with the same parameters as above using Eq. 32 of Hameury et al. 1998 ; see Fig. 2 of Lasota 2001 for a discussion of the importance of convection on  $\Sigma_{\max}$ ). Much higher densities can be reached on the cold branch and hence higher torques can be achieved during the evolution for the same  $\delta$  and  $\alpha$ . On the other hand, the approximate treatment for the response of the donor to mass loss for the binary evolution in the present calculation may artificially decrease the minimum  $\delta$  needed to have a dominant CB torque.

#### 4.3. Can CB disks become thermally unstable ?

Depending upon the evolution of the CB disk,  $\Sigma_i$  may become higher than the critical column density,  $\Sigma_{\max}$ , above which a cold, optically thick and geometrically thin disk becomes thermally and viscously unstable. The instability is due to the large change in opacity which accompanies hydrogen ionization (see Lasota 2001 for a review). Such a CB disk would present limit cycle oscillations analogous to those which occur in the accretion disks of dwarf novae.

While the linear stability problem is the same for the accretion disk and the CB disk, one should expect some differences to show up in the nonlinear development. In the accreting case, the increased mass flux in the hot state propagates inward into a decreasing volume, amplifying its effects. The instability in a CB disk starts at the inner edge and propagates outward into an increasing volume. One might thus expect its effects to be milder, and the transition front to stall at some moderate distance from the inner edge. To check on these expectations we have followed the instability in a few cases. But first, we investigate for which parameters the evolving binary with a CB disk can reach instability.

We combine the expression for  $\Sigma(R_i, t)$  (Eq. 3) with that for  $\Sigma_{\max}$  (Eq. 32 of Hameury et al. 1998) to estimate the time needed to reach this critical density, assuming the binary evolution is frozen (constant  $R_i$  and  $\dot{M}_i$ ). The central temperature at the critical density is  $T_c \approx 20000 \text{ K}$  (Hameury et al. 1998). We use this temperature to get an estimate of  $\nu_i \approx \alpha c_s^2 / \Omega_K$ , where  $c_s^2$  and  $\Omega_K$  are respectively the sound speed and Keplerian frequency at the inner edge. We find

$$t \approx 6 \times 10^{10} \alpha_{0.001}^{-0.7} M_1^{-1.2} \dot{M}_{i,14}^{-2} R_{i,11}^{5.7} \text{ years} \quad (5)$$

where  $\alpha$  is in units of 0.001,  $\dot{M}_i$  is in units of  $-10^{14} \text{ g s}^{-1}$ ,  $M$  is in solar masses and  $R_i$  is in units of  $10^{11} \text{ cm}$ . The results from a few numerical tests show a shallower dependence on  $\dot{M}_i$  (-1 instead of -2) but this is still a fair order-of-magnitude approximation. The steep dependence on  $R_i$  implies that instability can be reached within a Hubble time only if the binary is sufficiently tight during most of its evolution.

In the calculations of Figs. 3-6, the CB disk never reaches the critical densities required to become unstable. For reasonable assumptions on  $M_1$  (0.6-1.0  $M_{\odot}$ ) and  $M_2$  (0.1-0.6  $M_{\odot}$ ) the CB disk has an initial  $R_i$  of  $\approx 0.01 \text{ AU}$  for which the critical density  $\Sigma_{\max}$  is of the order of  $10^5 \text{ g cm}^{-2}$  for  $\alpha = 0.001$ . The density in the disk does not build up fast enough to trigger the instability before the binary starts evolving away from the initial conditions. Unrealistically high values of  $\delta \gtrsim 0.1$  would be required to quicken the density buildup. At these rates, the binary would also dissolve in a very short time.

If magnetic braking dominates during the evolution, the CB disk is necessarily not very massive and  $\Sigma_i$  stays far from its critical value. If the disk torque dominates, the mass transfer rate and  $\Sigma_i$  increase quickly, particularly during the runaway. However, under the present assumptions, the secondary expands as it rapidly sheds mass onto the white dwarf (Eq. 14 of Spruit & Ritter 1983). The runaway is thus accompanied by an increase of the orbital period, and hence of  $R_i$  (see Fig. 3), which prevents  $\Sigma_i$  from becoming greater than  $\Sigma_{\max}$  ( $\propto R_i$ ).

The adiabatic mass-radius exponent is -1/3 for a sequence of homologous stars; in this respect they behave like convective stars (Spruit & Ritter 1983). This limits the freedom of the model. We have relaxed this in a test calculation in which the mass-radius coefficient of -1/3 as it appears in the model was increased to +1/2. The other parameters are  $\alpha = 0.005$  and  $\delta = 0.005$  (Fig. 7). The global evolution is very similar to the one shown in Fig. 4 except that the secondary contracts in response to the runaway mass transfer at  $t \approx 30 \text{ Myr}$ . The orbital period decreases to  $\sim 2$  hours, bringing the inner edge of the CB disk to  $0.007 \text{ AU}$  ( $M_2 \approx 0.085 M_{\odot}$ ,  $R_2 \approx 0.16 R_{\odot}$ ). The inner column density  $\Sigma_i$  is then greater than the critical density and the CB disk, which is now  $\sim 0.003 M_{\odot}$ , becomes unstable.

We assume that, when the CB disk is hot, the viscosity coefficient  $\alpha_{\text{hot}}$  increases to 0.01 by analogy with the models of dwarf novae outbursts. The inner region of the CB disk cycles between a hot and a cold state in a complex fashion on a timescale of  $\sim 15$  years, with the hot state lasting about a year (see Fig. 7). Changes in the CB disk on such a short time scale do not translate into the mass transfer rate, which changes only on time scales of the order the ratio of the scale height of the stellar atmosphere to its radius times  $t_w$ . The mass transfer rate is therefore kept fixed at its current value when the instability starts ( $\dot{M}_2 \approx 2.4 \times 10^{-7} M_{\odot} \text{ yr}^{-1}$ ).

The instability would therefore only show up, if at all, as a brightening of the system in the near-infrared. The CB disk can indeed become very bright with a bolometric luminosity increasing by almost an order of magnitude to about  $2 \times 10^{34} \text{ erg s}^{-1}$ . The bolometric luminosity is calculated assuming the optically thick regions of the disk radiate as a blackbody and that the disk is seen face-on. Fig. 8 shows the evolution of the CB disk during the rise to the high luminosity state. A front develops at the inner unstable radius and propagates outward, transporting matter to larger radii and gradually heating the inner regions to mid-plane temperatures reaching  $10^5 \text{ K}$ . This is analogous to an outside-in outburst in a dwarf novae accretion disk, where the outer (tidally truncated) radius

becomes unstable first and a front propagates in the direction of the flow. However, in the CB case, the front stalls quickly due to the combination of the higher critical density needed to heat the disk and lower available density to do this (dilution into a larger volume of the transported mass). In contrast, a dwarf novae outside-in front heats the entire accretion disk because of the decreasing  $\Sigma_{\max}$  and volume at smaller radii. At the luminosity maximum, only the inner 0.02 AU are hot compared to the total (optically thick) CB disk size of 2.5 AU.

Our choice of boundary condition precludes the possibility of mass flow to the secondary. This may not be exact during outburst when the inner region becomes sufficiently thick ( $H/R \gtrsim 0.05$ ) that some matter may flow from the CB disk back to the companion star (Artymowicz & Lubow 1996). Such flows are non axisymmetric and their inclusion is beyond the scope of our simplified one dimensional radial description of the vertically integrated structure. Note that these flows are unlikely to change our conclusions on the possibility of having outbursts in CB disks.

## 5. SPECTRAL ENERGY DISTRIBUTIONS

Since the temperatures, densities, and size of the CB disk vary with time, the spectral appearance will depend upon the evolutionary stage of the binary system. The energy distributions for a CB disk viewed normal to its surface for three model sequences are illustrated in Figs. 9-11 assuming a distance of 100 pc. The distributions are shown for the CB disk early in the evolution, prior to, and during the accelerated mass transfer phase. In these calculations the disk surface is assumed to emit black body radiation at its effective temperature. This should be a reasonable approximation since the frequency dependence of the opacities (see Bell et al. 1997) show the CB disk to be optically thick to radiation at wavelengths  $\lesssim 350\mu\text{m}$ . The figures show the integrated flux over the optically thick parts of the disk.

It is seen that the continuum peaks in the near-infrared at  $\lambda \sim 3\mu\text{m}$  for the models sequences during the entire binary evolution. There is a tendency for the flux to increase for the more advanced evolutionary phases, when CB disks are larger and more massive. However, the flux does not increase at all wavelengths. The flux at  $\lambda \lesssim 3\mu\text{m}$  can decrease even though the mass input rate into the CB disk increases (see Fig. 9). This is due to the increase of the binary orbital separation in the accelerated evolution phase, causing the radiating surface area to increase and the temperatures in the inner regions to decrease. These results taken together indicate that the spectral energy distributions are not sensitive to  $\alpha$  and  $\delta$  in the range of 0.001 - 0.005.

To determine the observability of such disks, the flux contributions from the donor star and a steady accretion disk surrounding the white dwarf star must be taken into account. As an illustration we take an evolution with  $\alpha = 0.005$ ,  $\delta = 0.005$ , and  $t_w = 2 \times 10^8$  yr at  $t = 5 \times 10^6$  yr. At that evolutionary phase, a secondary of mass equal to  $0.36 M_\odot$  transfers matter to the white dwarf of mass equal to  $1.14 M_\odot$  at the rate of  $1.3 \times 10^{18} \text{ g s}^{-1}$ . We assume that the outer radius of the accretion disk is 0.67 times the Roche lobe radius of the white dwarf. The luminosity and effective temperature of the secondary are  $1.1 \times 10^{-3} L_\odot$

and 3500 K respectively, the values for a main sequence star of the same mass. Assuming a main sequence secondary is likely to overestimate the contribution from the donor star, which is not in thermal equilibrium because of the mass transfer. In Fig. 12 the spectral energy distribution from a steady state accretion disk and the low mass secondary component are included with the contribution from the CB disk. It is evident that the contribution of the CB disk increases with wavelength, and exceeds that due to the accretion disk and donor by a factor of about 20 and 400 at  $10 \mu\text{m}$  and  $350\mu\text{m}$  respectively. For wavelengths where the CB disk dominates the wavelength dependence is,  $F_\lambda \sim \lambda^{-2.6}$ . The radius enclosing 90% of the total flux emitted by the CB disk is  $\sim 5 \times 10^{11} - 1.6 \times 10^{12}$  cm at  $10\mu\text{m}$  and  $10^{12} - 10^{13}$  cm at  $100\mu\text{m}$ . Hence, the cool outer regions of the CB disk at  $R \gtrsim 5 \times 10^{11}$  cm provide the infrared and submm waveband signatures of its presence. We point out that the neglect of irradiation effects by the secondary is not expected to significantly modify this result since its importance in the outer parts of the disk (as inferred from the variation of  $H/R$  with respect to radius) is diminished by the shadowing effect by the innermost regions. We note, however, that the actual height of the disk differs from that estimated by the pressure scale height and irradiation effects of the outermost regions could be important (see Chiang & Goldreich 1997). In this case the infrared and sub mm fluxes would be increased and, hence, the fluxes estimated from the CB disk in the absence of irradiation effects should be considered a lower bound.

## 6. CONCLUSIONS

The evolution of a CB disk has been investigated for cases where it significantly accelerates the binary evolution, such that the mass transfer rate onto the white dwarf can reach  $\dot{M} \gtrsim 10^{-8} M_\odot \text{ yr}^{-1}$ , representative of nova-like variables and super soft sources. The column densities and temperatures in these disks are found to be similar to those in circumstellar (CS) disks surrounding young stellar objects. The column densities decrease with radius and reach maxima in the innermost regions of the disk with  $\Sigma_{\max}$  ranging up to  $4 \times 10^4 \text{ g cm}^{-2}$ . The midplane temperatures range from  $\sim 3500$  K at the inner edge to less than about 30 K in the optically thin outer regions. In contrast to the CS disks, where accretion can take place steadily, the outflowing mass in CB disks is distinctly non-steady. The outer boundary of the CB disk,  $R_d$ , increases with time (roughly as  $R_d \sim t^{1/2}$ ). We find that CB disks around CVs should extend to several AU, about 100 times smaller than CS disks.

The numerical results show that the fractional mass input rate into the CB disk required to accelerate the evolution is lower than found in Taam & Spruit (2001). This is due to the effect of convection on the disk structure (ignored in Taam & Spruit), which causes the lower stable branch of the  $\nu - \Sigma$  relation to extend to much higher column densities.

We find that the CB disks can become thermally unstable, but only under rather special conditions, namely at high mass transfer rates combined with short orbital periods. Such conditions could be met in the short period double degenerate AM CVn systems or, in a different

context, in disks around Be stars (Lee et al. 1991). For normal CVs, we find that the CB disk is unlikely to become unstable because of the long timescale needed to reach the critical column density. However, depending upon the response of the secondary to mass loss, the CB disk could become unstable during the accelerated evolution. If the CB disk is unstable, a heat front develops and propagates outward from the inner radius. In contrast to the accretion disks in dwarf novae, the heating front is quenched quickly because of the difficulty in raising the lower column densities encountered at larger radii to the increasing critical column densities needed to sustain propagation. The inner region cycles between the hot and cold states on a timescale of tens of years, inducing changes in the bolometric luminosity of a factor  $\sim 10$ .

We find that the spectral energy distributions expected of CB disks in CVs can dominate the emission from the donor star and the accretion disk of the white dwarf at wavelengths  $\lambda \gtrsim 3\mu\text{m}$ . At longer wavelengths the relative contribution from the CB disk to the total emission from the system increases.

Typical flux levels for a nova-like variable for an assumed distance of 100 pc would be about 0.3 Jy at  $10\mu\text{m}$  and a factor of 10 lower at  $450\mu\text{m}$ . Although the distances to CV's are not well known, the model calculations suggest that even in nova-like variables with distances order of 1 kpc, detection of CBs in the  $10 - 20\mu\text{m}$  region should be possible using the infrared detectors on the Gemini Observatory (Telesco et al. 2001) and the Keck Observatory (Jones et al. 1998). Although the emission from these

CB disks becomes optically thin at  $350\mu\text{m}$ , it is possible that the longer wavelength radiation at  $450\mu\text{m}$  may be detectable using the SCUBA instrument.

In our interpretation the nova-like variables would be CVs with mass transfer accelerated by a CB disk, which makes them natural targets for searches for CB disks. However, the predicted emission from the CB disk before the accelerated phase is similar, for a substantial period of time, to that during the accelerated phase. The possibility for their detection is therefore not limited to the systems with high mass transfer rates. We speculate that the 'extra infrared components' discovered by Harrison et al. (2000) in several well studied dwarf novae may in fact be due to CB disks. These observations show that searches of CB disks surrounding bright cataclysmic variable systems are technically possible with current instrumentation.

We thank T. Currie for his assistance in this study and J.-P. Lasota for useful discussions. In addition, we thank the referee, Dr. Kristen Menou, for his report which has improved the clarity of the manuscript. This research was supported in part by the National Science Foundation under Grant No. AST-9727875 and by NASA under the National Space Grant College and Fellowship Program. GD acknowledges support from NASA grants NAG 5-7007 and NAG 5-7034. HS acknowledges support from the European Commission under TMR grant ERBFMRX-CT98-0195 ('Accretion onto Black Holes, Compact Objects and Protostars').

#### REFERENCES

- Artymowicz, P., & Lubow, S.H. 1994, *ApJ*, 421, 651  
 Artymowicz, P., & Lubow, S.H. 1996, *ApJ*, 467, L77  
 Bell, K. R., Cassen, P. M., Klahr, H. H., & Henning, Th. 1997, *ApJ*, 486, 372  
 Bjorkman, J.E., & Cassinelli, J.P. 1993, *ApJ*, 409, 429  
 Bjorkman, J.E., & Wood K. 1995, *BAAS*, 27, 841  
 Chiang, E. I., & Goldreich, P. 1997, *ApJ*, 490, 368  
 Deufel, B., Barwig, H., Simic, D., Wolf, S., & Drory, N. 1999, *A&A*, 343, 455  
 Fromang, S., Terquem, C., & Balbus, S. A. 2002, *MNRAS*, 329, 18  
 Gammie, C. F., & Menou, K. 1998, *ApJ*, 492, L75  
 Hameury, J. M., Menou, K., Dubus, G., Lasota, J. P., & Hure, J. M. 1998, *MNRAS*, 298, 1048  
 Harrison, T. E., McNamara, B. J., Szkody, P., & Gilliland, R. L. 2000, *AJ*, 120, 2649  
 Hellier, C. 2000, *NewAR*, 44 131  
 Henning, Th., & Stognienko, R. 1996, *A&A*, 311, 291  
 Jones, B., Puetter, R. C., Smith, H. E., Stein, W. A., Wang, M. C., & Campbell, R. 1998, *BAAS*,  
 Lasota, J.-P. 2001, *New AR*, 45, 449  
 Lee, U., Saio, H., & Osaki, Y. 1991, *MNRAS*, 250, 432  
 Pringle, J. E. 1991, *MNRAS*, 248, 754  
 Shakura, N. I., & Sunyaev, R. A. 1973, *A&A*, 24, 337  
 Solheim, S.-E., & Sion, E. M. 1994, *A&A*, 287, 503  
 Spruit, H.C., & Ritter, H. 1983, *A&A*, 124, 267  
 Spruit, H. C., & Taam, R. E. 2001, *ApJ*, 548, 900  
 Taam, R. E., & Spruit, H. C. 2001, *ApJ*, 561, 329  
 Telesco, C. M., Pina, R. K., & Fisher, R. S. 2001, *BAAS*, 33, 814  
 Thorstensen, J.R., Ringwald, F.A., Wade, R.A., Schmidt, G.D., & Norsworthy, J.E. 1991, *AJ*, 102, 272

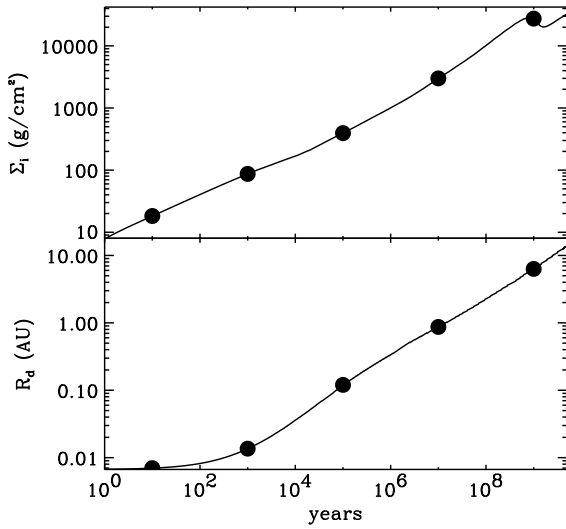


FIG. 1.— The evolution of a model CB disk with constant mass input rate ( $\dot{M}_i = -10^{14} \text{ g s}^{-1}$ ) and inner radius ( $R_i = 10^{11} \text{ cm}$ ), for viscosity parameter  $\alpha = 0.001$ . Top panel: column density at the inner disk edge  $\Sigma_i$ . Bottom panel: outer radius of the disk defined as the radius where the optical depth  $\tau = 1$ . The radial structure at the times indicated by the dots on these curves are presented in Fig. 2. The surface density required for disk-instability ( $\Sigma_{\text{max}} \approx 6 \times 10^4 \text{ g cm}^{-2}$  in this case) is not reached.

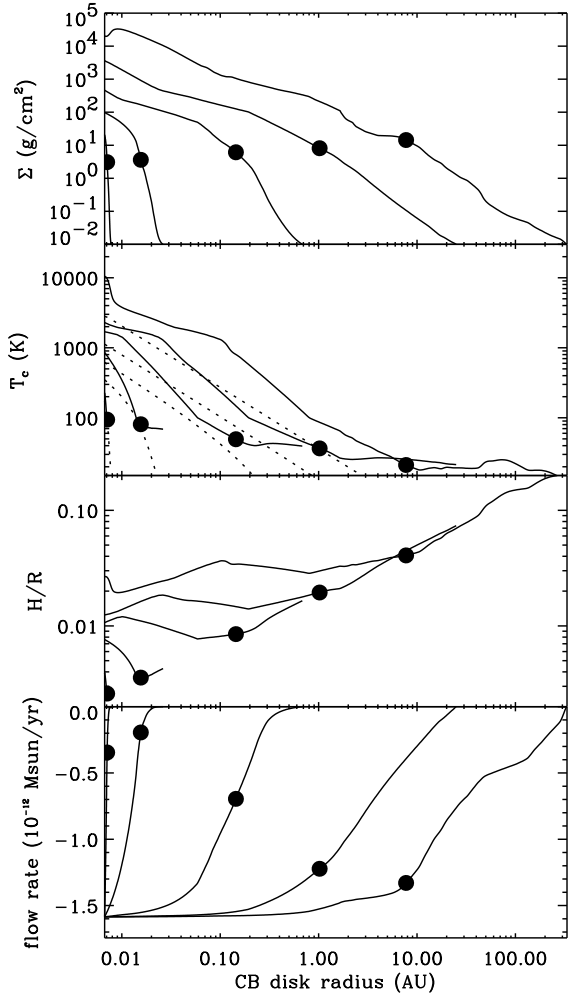


FIG. 2.— The radial structure of the CB disk presented in Fig. 1 at different times during its evolution. The column density,  $\Sigma$ , mid-plane temperature  $T_c$  (solid line), effective temperature  $T_{\text{eff}}$  (dashed line), ratio of pressure scale height to radius,  $H/R$ , and mass flow rate  $\dot{M}$  (in units of  $10^{-12} M_{\odot} \text{ yr}^{-1}$ , negative values indicate mass is flowing away from the binary) are illustrated as a function of radius and time (each radial curve corresponds to a dot in Fig. 1). The radius at which the optical depth equals 1 is marked by a dot on each curve.



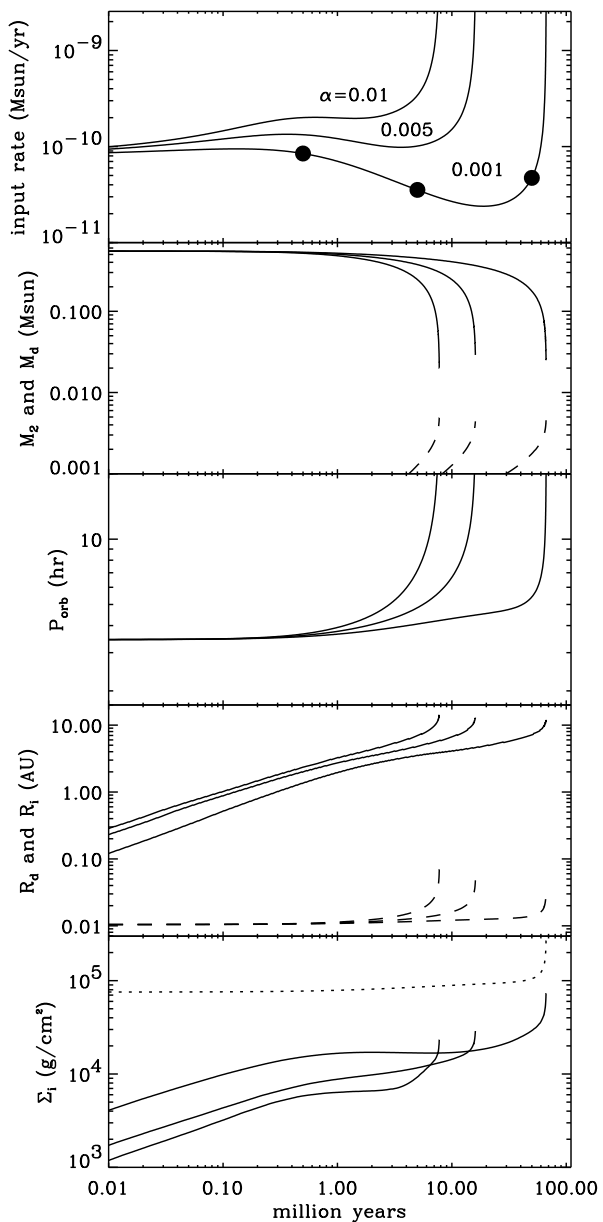


FIG. 3.— Evolution of the CB disk with the evolution of and angular momentum loss from the binary system taken into account. Three calculations are shown in each panel for values of the viscosity parameter  $\alpha = 0.01, 0.005$  and  $0.001$ . The calculations start with a secondary mass of  $0.55 M_{\odot}$  and a white dwarf of  $0.95 M_{\odot}$ . Viscosity parameter is  $\alpha = 0.001$ , time scale for angular momentum loss by magnetic braking of the binary is  $t_w = 2 \times 10^8$  years, and mass fed into the CB disk  $-\dot{M}_i$  is a fraction  $\delta = 0.005$  of the mass transfer rate. From top to bottom: the mass input rate into the CB disk  $-\dot{M}_i$ ; the mass of the secondary and the mass of the disk (dashed line); the orbital period; the outer radius of the CB disk (at which the optical depth equals 1) and the inner radius of the CB disk (dashed line); the column density at the inner disk edge  $\Sigma_i$  and the corresponding critical column density  $\Sigma_{\max}$  above which local thermal instabilities are expected (dashed line). The radial structure of the CB disk is shown at different times (indicated by the dots in the first panel) in Fig. 4.

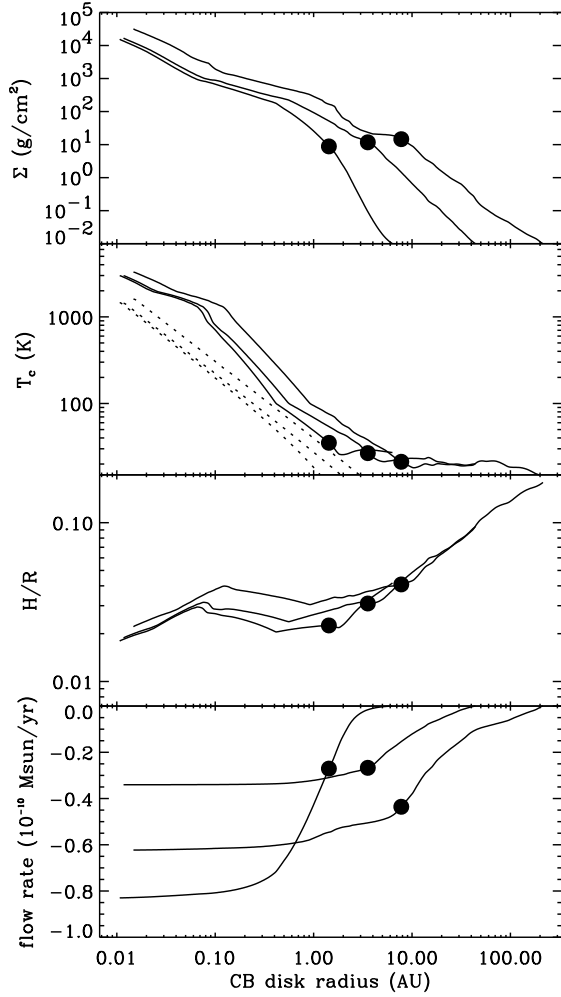


FIG. 4.— The radial structure of the CB disk with  $\alpha = 0.001$  presented in Fig. 3, at different times during its evolution. The column density  $\Sigma$ , the mid-plane temperature  $T_c$  (solid line) and the effective temperature  $T_{\text{eff}}$  (dashed line), the ratio of the pressure scale height to radius  $H/R$ , and the mass flow rate  $\dot{M}$  (in units of  $10^{-10} M_{\odot} \text{ yr}^{-1}$ ) are shown as functions of radius and time (at  $t = 5 \times [10^5, 10^6, 10^7]$  years, see Fig. 3). The radius at which the optical depth  $\tau = 1$  is shown as a dot on each curve.

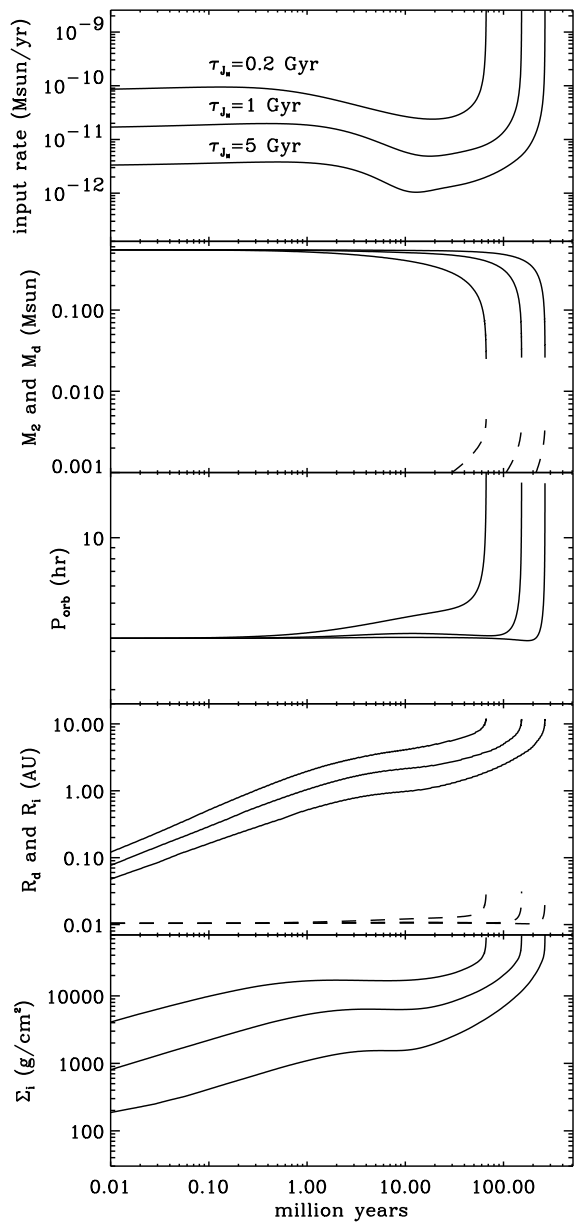


FIG. 5.— Same as Fig. 3 but showing the influence of varying  $t_w$ , the timescale for binary angular momentum loss by magnetic braking. The other parameters are  $\alpha = 0.001$  and  $\delta = 0.005$  and the calculations start with a secondary mass of  $0.55 M_{\odot}$  and a white dwarf of  $0.95 M_{\odot}$ .

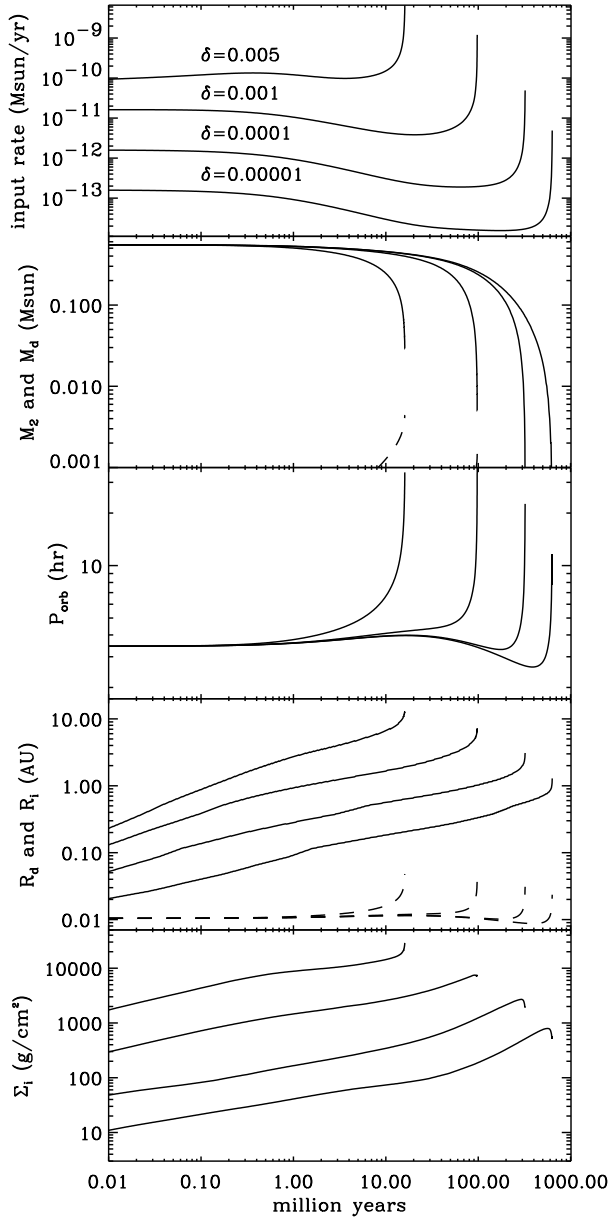


FIG. 6.— Same as Fig. 3 but showing the influence of varying  $\delta$ , the fraction of the binary mass transfer rate which is input in the CB disk. The other parameters are  $\alpha = 0.005$  and  $t_w = 2 \times 10^8$  years and the calculations start with a secondary mass of  $0.55 M_\odot$  and a white dwarf of  $0.95 M_\odot$ .

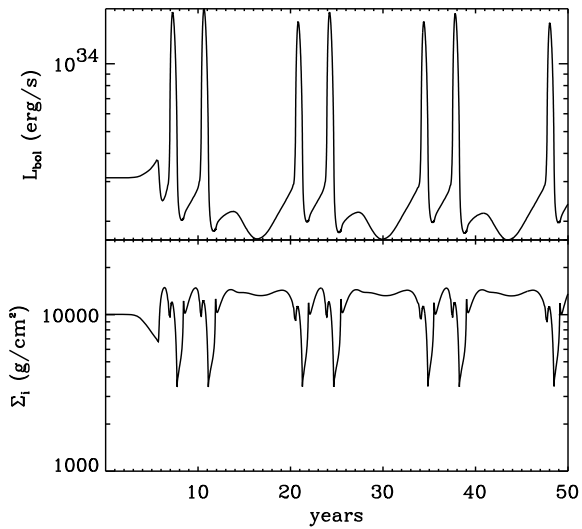


FIG. 7.— Example of a thermally and viscously unstable CB disk. The calculation starts with a  $0.55 M_{\odot}$  secondary and a  $0.95 M_{\odot}$  primary. We assume the secondary *contracts* in response to mass transfer (see §4.3),  $\alpha_{\text{cold}} = 0.005$ ,  $\alpha_{\text{hot}} = 0.01$  and  $\delta = 0.005$ . The evolution up to  $t \approx 30$  Myr is comparable to the model shown in Fig. 3. During the runaway, the radius of the secondary shrinks to  $0.16 R_{\odot}$ , decreasing the orbital period to  $\approx 2$  hours and bringing the CB disk to shorter radii (0.007 AU). The critical  $\Sigma_{\text{max}}$  is then low enough for the disk to become unstable. The upper and lower panels show the bolometric luminosity and the column density at the inner edge of the CB disk after it becomes unstable. The mass input into the disk is constant during the cycles at  $-\dot{M}_i \approx 10^{-9} M_{\odot} \text{ yr}^{-1}$ . The evolution of the radial structure of the CB disk for the outburst at  $t \approx 24$  yrs is shown in Fig. 8.

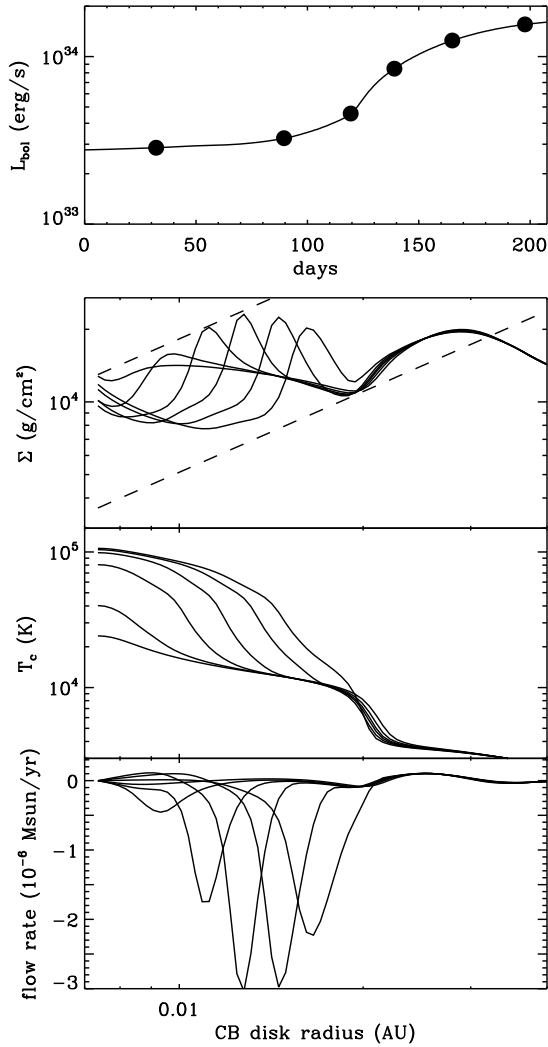


FIG. 8.— Evolution of the radial structure of a CB disk during the rise to a luminous state. The model shown is that of Fig. 7 for the outburst peaking at  $t \approx 24$  yrs. The top panel is a zoom on the bolometric luminosity lightcurve with the dots indicating at which times the 6 radial structures shown underneath were taken. The bottom three panels show the radial profiles of the column density  $\Sigma$ , mid-plane temperature  $T_c$  and mass flow rate in the CB disk  $\dot{M}$  (in units of  $10^{-6} M_{\odot} \text{ yr}^{-1}$ ). The two dashed lines in column density panel are the critical densities  $\Sigma_{\text{max}}$  (top) and  $\Sigma_{\text{min}}$  (bottom). In contrast to the outbursts in standard *accretion* disks, the front does not propagate very far out into the CB disk before it stalls.

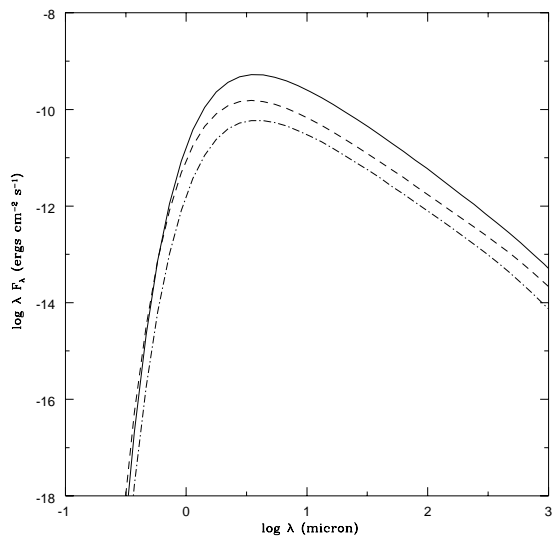


FIG. 9.— The spectral energy distribution for a CB disk for the model sequence with  $\alpha = 0.001$  and  $\delta = 0.005$  for an assumed distance of 100 pc. The dash - dot curve, dashed curve, and solid curve show stages of evolution at  $t = 5 \times 10^6$  yr,  $5 \times 10^7$  yr, and  $7 \times 10^7$  yr respectively.

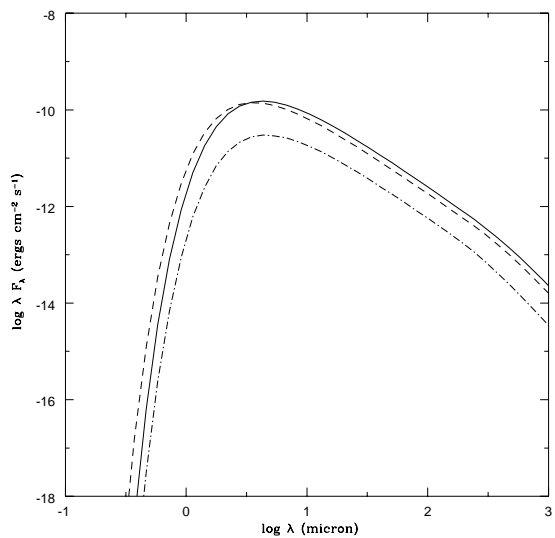


FIG. 10.— The spectral energy distribution for a CB disk for the model sequence with  $\alpha = 0.005$  and  $\delta = 0.001$  for an assumed distance of 100 pc. The dash - dot curve, dashed curve, and solid curve show stages of evolution at  $t = 8 \times 10^6$  yr,  $8 \times 10^7$  yr, and  $9 \times 10^7$  yr respectively.

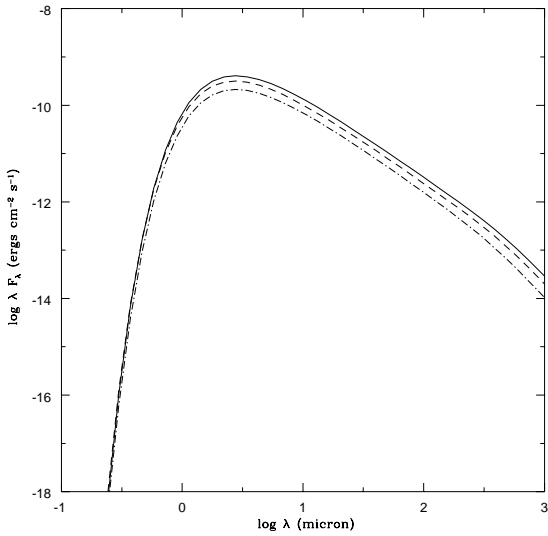


FIG. 11.— The spectral energy distribution for a CB disk for the model sequence with  $\alpha = 0.005$  and  $\delta = 0.005$  for an assumed distance of 100 pc. The dash - dot curve, dashed curve, and solid curve show stages of evolution at  $10^6$  yr,  $5 \times 10^6$  yr, and  $9 \times 10^6$  yr respectively.

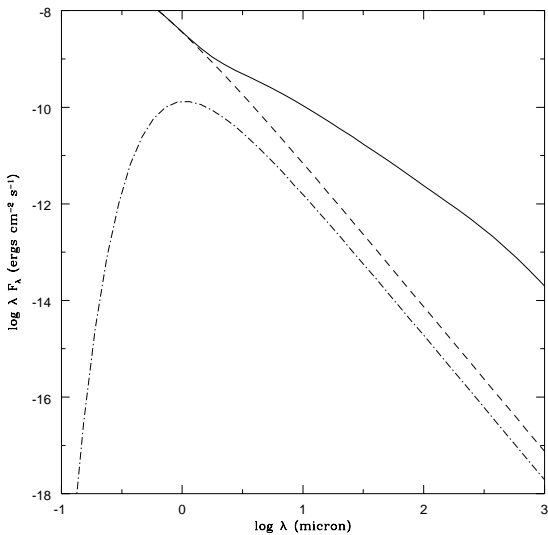


FIG. 12.— The spectral energy distribution for a cataclysmic variable system with CB disk, for  $\alpha = 0.005$  and  $\delta = 0.005$  at an evolutionary time of  $5 \times 10^6$  yr. At this time,  $\dot{M}_2$ , is  $1.3 \times 10^{18} \text{ g s}^{-1}$ . The distance is assumed equal to 100 pc. The dash - dot curve shows the contribution from a low mass secondary star of mass  $0.36 M_{\odot}$ , the dashed curve corresponds to the sum of the contribution from a steady state accretion disk surrounding the white dwarf component of mass  $1.14 M_{\odot}$  and the low mass secondary, and the solid curve includes the contribution from the CB disk as well. Note that the CB disk dominates the spectral energy distribution for  $\lambda \gtrsim 3 \mu\text{m}$ .